

HUBBLE IMAGING OF THE IONIZING RADIATION FROM A STAR-FORMING GALAXY AT  $Z = 3.2$  WITH  $F_{\text{ESC}} > 50\%$ 

E. VANZELLA<sup>1,\*</sup>, S. DE BARROS<sup>1</sup>, K. VASEI<sup>2</sup>, A. ALAVI<sup>2</sup>, M. GIAVALISCO<sup>3</sup>, B. SIANA<sup>2</sup>, A. GRAZIAN<sup>4</sup>, G. HASINGER<sup>5</sup>, H. SUH<sup>5</sup>, N. CAPPELLUTI<sup>6</sup>, F. VITO<sup>7</sup>, R. AMORIN<sup>4</sup>, I. BALESTRA<sup>8,9</sup>, M. BRUSA<sup>10,1</sup>, F. CALURA<sup>1</sup>, M. CASTELLANO<sup>4</sup>, A. COMASTRI<sup>1</sup>, A. FONTANA<sup>4</sup>, R. GILLI<sup>1</sup>, M. MIGNOLI<sup>1</sup>, L. PENTERICCI<sup>4</sup>, C. VIGNALI<sup>10</sup> AND G. ZAMORANI<sup>1</sup>

## ABSTRACT

Star-forming galaxies are considered to be the leading candidate sources that dominate the cosmic reionization at  $z > 7$ , and the search for analogs at moderate redshift showing Lyman continuum (LyC) leakage is currently a active line of research. We have observed a star-forming galaxy at  $z = 3.2$  with *Hubble*/WFC3 in the F336W filter, corresponding to the 730-890Å rest-frame, and detect LyC emission. This galaxy is very compact and also has large Oxygen ratio  $[\text{OIII}]\lambda 5007/[\text{OII}]\lambda 3727 (\gtrsim 10)$ . No nuclear activity is revealed from optical/near-infrared spectroscopy and deep multi-band photometry (including the 6Ms X-ray *Chandra*). The measured escape fraction of ionizing radiation spans the range 50-100%, depending on the IGM attenuation. The LyC emission is detected with  $m_{\text{F336W}} = 27.57 \pm 0.11$  (S/N=10) and it is spatially unresolved, with effective radius  $R_e < 200\text{pc}$ . Predictions from photoionization and radiative transfer models are in line with the properties reported here, indicating that stellar winds and supernova explosions in a nucleated star-forming region can blow cavities generating density-bounded conditions compatible with optically thin media. Irrespective to the nature of the ionizing radiation, spectral signatures of these sources over the entire electromagnetic spectrum are of central importance for their identification during the epoch of reionization, when the LyC is unobservable. Intriguingly, the *Spitzer*/IRAC photometric signature of intense rest-frame optical emissions ( $[\text{O III}]\lambda\lambda 4959, 5007 + \text{H}\beta$ ) observed recently at  $z \simeq 7.5 - 8.5$  is similar to what is observed in this galaxy. Only the *James Webb Space Telescope* will measure optical line ratios at  $z > 7$  allowing a direct comparison with lower redshift LyC emitters, as reported here.

*Subject headings:* galaxies: evolution — galaxies: high-redshift — dark ages, reionization, first stars

## 1. INTRODUCTION

Cosmic reionization is a major episode in the history of the Universe and the search for ionizing sources is one of the main goals of modern observational cosmology (Robertson et al. 2010). Star-forming galaxies and AGN have been proposed to be the dominant sources of ionizing radiation, possibly acting at different cosmic epochs (Haardt & Madau 2012). While the redshift evolution of the ultraviolet luminosity function of star-forming galaxies is relatively well measured up to  $z \simeq 7 - 8$ , showing that the bulk of the ultraviolet luminosity density is dominated by the faint galaxy population ( $L < L^*$ , e.g. Bouwens et al. 2015), the number density of high redshift and faint AGN is still highly uncertain (e.g., Giallongo et al. 2015; Georgakakis et al. 2015). In addition, understanding the mechanisms of reionization (and post-reionization  $z < 6$ )

hinges on understanding how the escape fraction of ionizing radiation,  $f_{\text{esc}}(\text{LyC})$ , changes as a function of luminosity and redshift. Because of the IGM opacity, direct observation of ionizing radiation during reionization is not feasible (Prochaska et al. 2010). A strategy to make progress is to identify LyC sources at lower redshift, e.g. 3-3.5, and study which of their properties can be used as predictors of a LyC leakage. Recent advances have been made by looking at starburst galaxies in the local universe (Borthakur et al. 2014; Izotov et al. 2016), about 10 Gyrs after reionization ended ( $z \sim 6$ ). However, it is more useful to identify LyC leakers at the highest redshifts possible ( $z \sim 3$ , one billion years after the end of reionization), because the properties of these galaxies are better analogs to those that reionized the universe.

Escaping LyC radiation from galaxies has been searched in the recent years (Vanzella et al. 2010a; Siana et al. 2010; Nestor et al. 2013; Mostardi et al. 2013, 2015) and, to date, no convincing LyC emission has been reported at high redshift (Siana et al. 2015). Moreover, nothing is known about the spatial distribution of the emerging LyC radiation. Here we report on a LyC emission arising from a distant galaxy ( $z = 3.212$ ) unambiguously confirmed with *HST* observations.

Throughout the paper, the AB system ( $AB = 31.4 - 2.5 \log(f_{\nu}/n\text{Jy})$ ) and cosmology  $\Omega_{\text{tot}}$ ,  $\Omega_M$ ,  $\Omega_{\Lambda} = 1.0, 0.3, 0.7$  with  $H_0 = 70\text{km s}^{-1}\text{Mpc}^{-1}$  are used.

## 2. THE CHALLENGING DETECTION OF ESCAPING LYC PHOTONS

The difficulty of directly and unambiguously identifying the LyC radiation in distant galaxies are due to a combination of several effects: (1) superposition of foreground sources can produce false LyC detections (Vanzella et al. 2010a, 2012), and in this respect *HST* observations are crucial (Siana et al. 2015); (2) the intergalactic transmission in the ionizing domain is stochastic (Inoue et al. 2014); (3) the geometrical

<sup>1</sup> INAF–Osservatorio Astronomico di Bologna, via Ranzani 1, 40127 Bologna, Italy

<sup>2</sup> Department of Physics and Astronomy, University of California, Riverside, CA 92507, USA

<sup>3</sup> Astronomy Department, University of Massachusetts, Amherst, MA 01003, USA

<sup>4</sup> INAF–Osservatorio Astronomico di Roma, via Frascati 33, 00040 Monteporzio, Italy

<sup>5</sup> Institute for Astronomy, 2680 Woodlawn Drive, Honolulu, HI 96822, USA

<sup>6</sup> Yale Center for Astronomy and Astrophysics, Physics Department, New Haven, CT 06520, USA

<sup>7</sup> Department of Astronomy and Astrophysics, 525 Davey Laboratory, The Pennsylvania State University, University Park, PA 16802, USA

<sup>8</sup> INAF - Osservatorio Astronomico di Trieste, via G. B. Tiepolo 11, I-34131, Trieste, Italy

<sup>9</sup> University Observatory Munich, Scheinerstrasse 1, D-81679 München, Germany

<sup>10</sup> Dipartimento di Fisica e Astronomia, Università degli Studi di Bologna, Viale Berti Pichat 6/2, 40127 Bologna, Italy

\* eros.vanzella@oabo.inaf.it

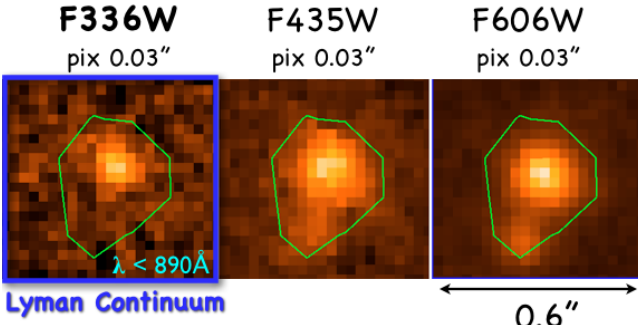


FIG. 1.— From left to right, the F336W, F435W and F606W *HST*/ACS thumbnails of *Ion2*. A LyC emission (rest-frame  $\lambda < 890\text{\AA}$ ) arising from the brighter component (A) is evident in the F336W-band images. The green iso-contour derived from the F435W band guides the eye in comparing the shape of the source. Secondary emission (B), offset by  $0.2''$ , is visible below the main source in the F435W and F606W images, but not in the F336W.

distribution of the neutral gas in galaxies and the relatively short duty cycle of  $f_{\text{esc}}(\text{LyC})$  over cosmic time adds further stochasticity in the LyC visibility (Wise et al. 2014; Cen & Kimm 2015); (4) the accessible luminosity range in the LyC achievable by current large telescopes limits the analysis to bright galaxies ( $L > 0.5L^*$ ) for which the average escaping ionizing radiation has now been shown to be intrinsically low ( $< 5 - 10\%$ , Grazian et al. 2016; Vanzella et al. 2010b; Mostardi et al. 2015; Siana et al. 2015). These aspects make the search for escaping ionizing radiation challenging and can explain the current low detection rate at high redshift. Nevertheless, the identification of examples with escaping LyC radiation lying in the tail of the large  $f_{\text{esc}}(\text{LyC})$  values, though rare (Vanzella et al. 2010b), represents the only empirical way we have to increase our physical insight into the mechanisms that allow ionizing photons to escape and thus providing unique reference for studies at  $z > 6$ .

### 2.1. The selected candidate LyC emitter

A LyC candidate at  $z = 3.212$  in the GOODS-Southern field, named *Ion2* (GDS-ID 033203.24-274518.8), was first identified by Vanzella et al. (2015). The compact star-forming region, showing strong  $[\text{O III}]\lambda\lambda 4959, 5007$  emission lines (with a rest-frame equivalent width of  $1500\text{\AA}$ ) and large Oxygen ratio  $[\text{OIII}]\lambda 5007/[\text{OII}]\lambda 3727 (\geq 10)$  makes *Ion2* the highest redshift “Green Pea” galaxy currently known and, accordingly to the photoionization models (Nakajima & Ouchi 2014; Jaskot & Oey 2013), an ideal candidate LyC emitter. A plausible spectroscopic LyC detection was subsequently discussed in de Barros et al. (2016). However, the presence of a close companion not resolved with ground-based spectroscopy and imaging ( $0.2''$ , see Fig. 1) casted some doubts about the association with *Ion2* of the observed flux and thus on the reliability of the LyC leakage.

### 3. HST OBSERVATIONS

To confirm the LyC emission, we obtained *HST* WFC3/UVIS image in the F336W filter, corresponding to rest-frame  $730 - 890\text{\AA}$ . Seventeen 2800s (1-orbit) dithered exposures were taken for a total integration time of 47.6 ks. The charge transfer efficiency (CTE) of the WFC3/UVIS CCDs has degraded significantly due to radiation damage and is particularly problematic in images with low background. To mitigate the effects of poor CTE, we increased the background

to  $\sim 12e^- \text{ pix}^{-1}$  with a post-flash LED (Biretta & Baggett 2013). Furthermore, we placed the target near the read-out edge of the CCD so that electrons need only transfer across  $\sim 300$  of the 2048 pixels. Finally, we applied a pixel-based CTE correction<sup>12</sup>. As the dark current is nearly half of the total background, proper dark subtraction is critical. Unfortunately, the STScI darks are only a single value and do not capture the gradient and blotchy pattern in the dark current (Teplitz et al. 2013). Also, because the darks are not CTE corrected, more than half of hot and warm pixels are not properly masked (Rafelski et al. 2015). To mitigate these issues we adopted the dark processing method explained in detail in Rafelski et al. (2015). First, we CTE-correct all raw dark images in the anneal cycle of our visits and remove the cosmic rays. We then find and mask the hot pixels that appear throughout the anneal cycle and make a mean super dark from all darks in the anneal cycle. We then dark subtract the science images while masking the hot pixels that were found to exist at the time of the observation.

We processed all of our CTE-corrected raw data using STS-DAS task CALWF3, including subtraction of our new super darks. These calibrated images were then combined using Astrodrizzle (Gonzaga & et al. 2012), which performs background subtraction, cosmic ray rejection and geometric distortion correction. The final combined F336W image has a pixel scale of  $0.03''$  and is astrometrically aligned with the 3D-HST F606W image (Skelton et al. 2014) with a precision of 48 mas. As a by-product, Astrodrizzle produces an inverse variance image used to derive the uncertainties in the photometry. We performed aperture photometry using a growth-curve methodology. The estimated uncertainty was corrected for the correlated noise introduced in the drizzling process (Casetano et al. 2000). Finally, we corrected our photometry for Galactic extinction (0.041 magnitude; Schlafly & Finkbeiner 2011).

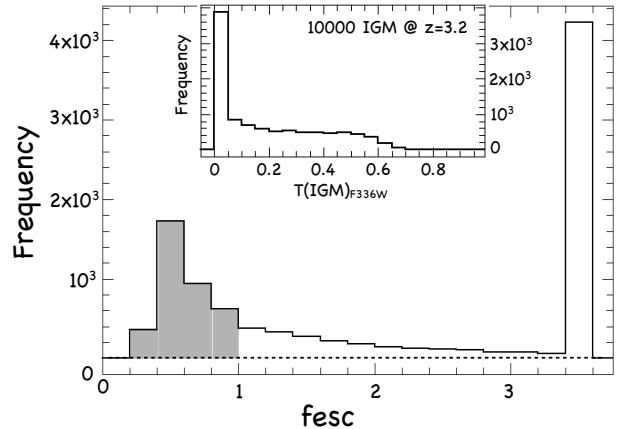


FIG. 2.— The distribution of  $f_{\text{esc}}(\text{LyC})$  is shown in the main panel adopting an intrinsic luminosity density ratio  $(L_{1500}/L_{800})_{\text{INT}} = 5$  (see Eq. 1). Values of  $f_{\text{esc}}(\text{LyC}) > 3.5$  have fixed to 3.5 to better display the entire distribution.  $f_{\text{esc}}(\text{LyC}) < 1$  corresponds to 37% of the 10000 realizations (gray histogram). The inset shows the IGM transmission at  $z = 3.2$  (from Inoue et al. (2014)). The F336W flux requires both a relatively high  $f_{\text{esc}}(\text{LyC}) (> 40\%)$  or small ratio  $(L_{1500}/L_{800})_{\text{INT}} < 10$ .

## 4. RESULTS

<sup>12</sup> [http://www.stsci.edu/hst/wfc3/tools/cte\\_tools](http://www.stsci.edu/hst/wfc3/tools/cte_tools)

The HST imaging clearly solved the problem of the close neighbour and the LyC emission has been unambiguously confirmed at  $S/N = 10$  with magnitude  $m(F336W) = 27.57 \pm 0.11$  (see Fig. 1). It also provides the spatial mapping of ionizing radiation from a galaxy for the first time. From deep multi-wavelength observations, including *Chandra* 6Ms image, *HST* optical (GOODS, Giavalisco et al. 2004) and near-infrared (CANDELS, Grogin et al. 2011), *Spitzer* (3.6, 4.5, 5.8, 8.0, 24  $\mu$ m) and wide spectroscopic coverage from  $U$  to the  $K$  band (VLT and Keck), we found *Ion2* to be a low-mass ( $\leq 10^9 M_{\odot}$ ), low-metallicity ( $\sim 1/6 Z_{\odot}$ ) star-forming galaxy (de Barros et al. 2016).

We derived the  $f_{\text{esc}}(\text{LyC})$  quantity with usual formulation (e.g., Vanzella et al. 2012):

$$f_{\text{esc}}(\text{LyC}) = \frac{(L1500/L800)_{\text{INT}}}{(f1500/f800)_{\text{OBS}}} \times \frac{1}{T(\text{IGM})_{F336W}} \times 10^{-0.4 \times A1500} \quad (1)$$

where  $f1500/f800$  is the observed flux density ratio ( $= 14.60$ ) and the dust attenuation  $A1500$  has been derived by de Barros et al. (2016) ( $E(B-V) < 0.04$ ,  $A1500 \simeq 0.4$ ). Fig. 2 shows the distribution of  $f_{\text{esc}}(\text{LyC})$  calculated adopting the intrinsic ratio  $(L1500/L800)_{\text{INT}} = 5$  (Siana et al. 2007) and convolving with 10000 IGM transmission at  $z = 3.2$  (Eq. 1). A  $f_{\text{esc}}(\text{LyC}) < 1$  is still possible if  $(L1500/L800)_{\text{INT}} < 15$  with a high  $T(\text{IGM})_{F336W}$  ( $\simeq 0.7$ ).

#### 4.1. The ionizing photon production rate

The measured ionizing photon production rate corresponding to the observed  $m(F336W) = 27.57$  is  $N_{\text{phot}}(800\text{\AA}) = 1.7 \times 10^{53} \text{s}^{-1}$ . The statistical error related to the measured magnitude is negligible if compared to the stochasticity of the IGM attenuation affecting a single line of sight, as shown by the distribution of F336W-IGM convolved transmissions derived from the IGM prescription of Inoue et al. (2014) ( $T(\text{IGM})_{F336W}$ , Fig. 2). Assuming the maximum  $T(\text{IGM})_{F336W}$  allowed at  $z = 3.2$  ( $\simeq 70\%$ ), we have an intrinsic  $m(F336W) = 27.18$  that corresponds to  $N_{\text{phot}}(800\text{\AA}) = 2.5 \times 10^{53} \text{s}^{-1}$ . We can set a conservative upper limit to  $N_{\text{phot}}$  by assuming that the intrinsic F336W magnitude (ionizing emission) cannot be brighter than the observed magnitude at 1500  $\text{\AA}$  rest-frame ( $\sim 24.66$ ), i.e. the intrinsic luminosity density ratio is  $L1500/L800 > 1$  (i.e., no extreme stellar populations are present). We obtain  $N_{\text{phot}}(800\text{\AA}) = 2.5 \times 10^{54} \text{s}^{-1}$ . Therefore the intrinsic ionizing photon production rate is  $2.5 \times 10^{53} \text{s}^{-1} \leq N_{\text{phot}}(800\text{\AA}) \leq 2.5 \times 10^{54} \text{s}^{-1}$ .

#### 4.2. LyC morphology

The LyC leakage is co-spatial with the component *A* and nothing is detected from component *B*, where *A* and *B* refer to the brighter and the fainter blobs, respectively (see Fig. 1, following the Vanzella et al. (2015) nomenclature). *Ion2* is a compact but well resolved galaxy in the F435W, F606W, F775W and F850LP ACS images, corresponding to the rest-frame far-UV from 1030 to 2020  $\text{\AA}$ . The galaxy, however, does not appear to be resolved in the WFC3 F336W image. We have a well-exposed nearby bright star and inserted in a blank area of the image at random position to simulate a number ( $N = 50$ ) of realizations of the PSF, after rescaling it to the same flux as *Ion2*. We have then registered the star at the same position of the light centroid of *Ion2* and subtracted it, in each case obtaining residuals consistent with the sky background

(an example is shown in Fig. 3). We have also compared the morphology of *Ion2* in the F336W and F435W bands to test the possibility that the lower SNR in the former band is the reason of the apparent unresolved morphology, adopting the following procedure. Basic PSF-corrected morphological information from both components were extracted by Vanzella et al. (2015) using GALFIT (Peng et al. 2010). Given their regular (symmetric) morphology, the GALFIT modeling with a Gaussian light profile well reproduces both regions in all the ACS images and shows they are spatially resolved with effective radii of a few hundred parsecs. In particular, we show in Fig. 4 the result obtained at 1000  $\text{\AA}$  rest-frame (F435W band) adopting a Gaussian shape. The best solution produces an effective radius of  $R_e = 340 \pm 25 \text{ pc}$ , suggesting the stellar radiation emerges from a compact and resolved region; the error has been calculated by running GALFIT on simulated images obtained by inserting the B-band model in random and free regions of the F435W-band image. GALFIT fitting on the LyC image does not produce resolved solutions. In order to characterize the LyC morphology we perform a simple test by subtracting the best-fit B435-band model from the F336W image. After normalizing the two images at the same flux peak and checking the residuals also over a grid of dimming factors, it turns out that the LyC emission arises from a region smaller than what has been inferred from the F435W band (see Fig. 3), in particular the spatially unresolved detection in F336W corresponds to an effective radius  $< 200 \text{ pc}$ . The negative residual flux seen in Fig. 3 extends at least 5 pixels radially from the center, and can't be explained by the small variations in the PSFs at the two wavelengths. The observed compactness of the LyC emission is probably not surprising if we compare our *HST* resolution to the size of the super-star clusters observed in local starbursts, in which the O-type stars are spatially segregated toward the center within tens of parsecs (e.g., Annibali et al. 2015; James et al. 2016).

Another possible interpretation is that the LyC emission of *Ion2* could originate from an AGN. This is unlikely and is discussed in Sect. 5.1.

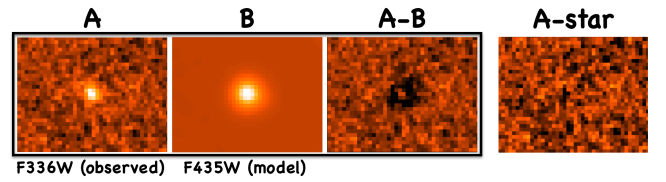


FIG. 3.— The difference between the observed F336W image (A) GALFIT best-fit model calculated in the F435W image (B) is shown in the right, (A-B). The model A is scaled to the flux peak of the F336W source (B). This comparison suggests the LyC emitting region is more compact than the resolved emission measured in the F435W band. In the right panel the residuals after subtracting a star rescaled to the source flux is shown. The size of the thumbnails is  $1.2'' \times 1.0''$ .

## 5. DISCUSSION

Independent from the nature of ionizing photons, the LyC detection implies a low column density of neutral gas along the line of sight, lower than  $10^{17.2} \text{ cm}^{-2}$  (corresponding to  $\tau(\text{LyC}) < 1$ ). de Barros et al. (2016) has shown for the first time empirical evidences linking high  $f_{\text{esc}}(\text{LyC})$  with compactness of the star-forming region, the large  $[\text{OIII}]/[\text{OII}]$  line ratio, the weak ultraviolet interstellar absorption lines, and the emerging  $\text{Ly}\alpha$  emission close to the systemic redshift, as predicted by photoionization and radiative transfer models when the medium is considered optically thin (Verhamme

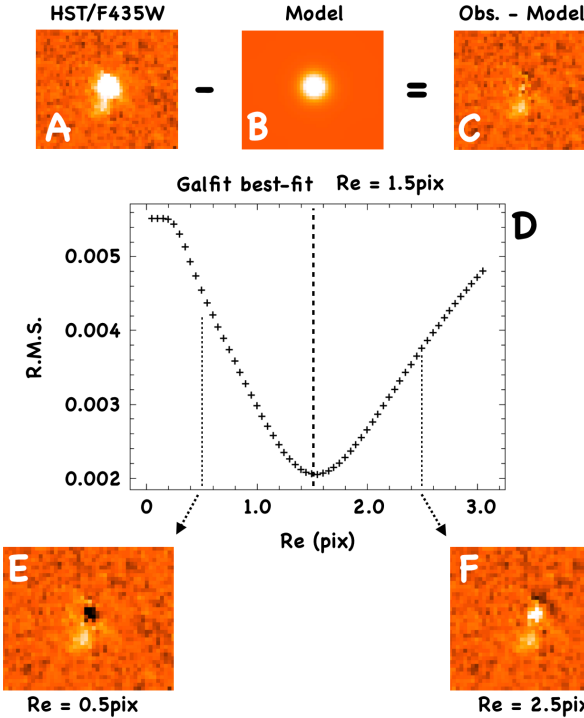


FIG. 4.— GALFIT modeling of the *Ion2* galaxy in the F435W band (1000Å rest-frame). In panel C the residuals of observed (A) - model (B) are shown for the best-fit case ( $R_e = 1.5\text{px} \simeq 340\text{pc}$ ). Bottom panels show an example of two “bad” solutions (observed-model), in which positive/negative residuals are evident (panels E/F). Middle panel (D) shows the behaviour of the r.m.s. calculated at the ‘A’ position by running GALFIT in a grid of effective radii (as described in Vanzella et al. (2015)). A good convergence is reached at  $R_e = 1.5 \pm 0.1\text{px}$ . This illustrates that the source is spatially resolved at 1000Å rest-frame. The size of the thumbnails is  $1.2'' \times 1.0''$ .

et al. 2015; Jaskot & Oey 2013; Borthakur et al. 2014; Nakajima & Ouchi 2014; Izotov et al. 2016). The *HST* observations presented here unambiguously confirm those predictions.

### 5.1. Nature of the source of the LyC photons

In the following, we summarize a few key elements (de Barros et al. 2016) and also add new empirical and theoretical evidence that favors the stellar origin of the ultraviolet light.

1. No high-ionization emission lines like  $\text{Nv}\lambda 1240$ ,  $\text{CIV}\lambda 1550$ ,  $\text{HeII}\lambda 1640$  have been detected at more than  $3\sigma$  level from the VLT/VIMOS MR spectrum (Fig. 5), while the  $\text{CIII}\lambda 1909$  line is clearly detected. From  $\text{CIV}\lambda 1550/\text{CIII}\lambda 1909 < 0.15$  and  $\text{CIII}\lambda 1909/\text{HeII}\lambda 1640 > 4.0$  line ratios and following Feltre et al. (2016), this source is classified as a star-forming galaxy, lying in the same region occupied by low-metallicity galaxies of Stark et al. (2014).

2. *Ion2* is spatially resolved in all of the ACS bands ( $340 \pm 25\text{pc}$ ) implying the stellar emission is detected and dominating the observed range 1000Å-2000Å rest-frame.

3. The narrow width of the  $[\text{OIII}]\lambda 5007$  emission line ( $\sigma = 65\text{km s}^{-1}$ ) is compatible with lower redshift star-forming galaxies (Maseda et al. 2014), while the AGN population typically show higher velocity dispersions up to several hundreds or thousand  $\text{km s}^{-1}$ .

4. *Ion2* is not detected in the X-ray in the 4 Ms CDFS (Cappelluti et al. (2015)) and no evidence of emission is inferred from the recent Chandra pointings publicly available on the Chandra website<sup>13</sup>, which increased the exposure time to  $\sim 6\text{Ms}$  (see Fig. 5). This places an X-ray luminosity limit of  $L_X \lesssim 3 \times 10^{42} \text{ ergs}^{-1}$  at  $1\sigma$  limit. If *Ion2* were a type I AGN, and assuming that the  $L_X - L_{[\text{OIII}]}$  relation observed locally is valid at  $z = 3$ , the measured  $[\text{OIII}]\lambda 5007$  luminosity (de Barros et al. 2016) would imply a detection with  $S/N > 100$  at the *Ion2* position in the 6Ms X-ray image, corresponding to  $L_X \simeq 10^{45} \text{ ergs}^{-1}$  (Panessa et al. 2006; Ueda et al. 2015). The measured  $[\text{OIII}]\lambda 5007$  line luminosity ( $2 \times 10^{43} \text{ ergs}^{-1}$ ) and the non detection in the 6Ms X-ray would imply a high obscuration (if it were an AGN), formally with an equivalent column density  $N_H > 10^{25} \text{ cm}^{-2}$  (assuming solar metallicity). The estimated stellar mass from the LyC source is  $\sim 10^8 \text{ M}_\odot$  (see Section 5.2) and, following Maseda et al. (2014), the dynamical mass from the  $[\text{OIII}]\lambda 5007$  line width ( $\sigma = 65 \text{ km s}^{-1}$ ) is  $\sim 10^9 \text{ M}_\odot$ . A lower limit on the BH mass of  $10^8 \text{ M}_\odot$  can be estimated by converting the  $[\text{OIII}]\lambda 5007$  line luminosity into an AGN bolometric luminosity (Panessa et al. 2006; Lusso et al. 2012) and then assuming that the AGN is radiating at the Eddington limit, that imply a very unusual and probably unrealistic ratio of  $M_{BH}/\text{Total mass} \geq 0.1$  for this object.

5. Adopting the expected  $L_X$  (from  $[\text{OIII}]\lambda 5007$  reported above), we expect a clear detection at  $6\mu\text{m}$  rest-frame (i.e., at  $24\mu\text{m}$  observed with *Spitzer*/MIPS) by assuming valid the relation between  $L_X$  and  $L(6\mu\text{m})$  (Stern 2015). In particular even adopting a  $L_X > 10^{44} \text{ erg s}^{-1}$  we expect  $L(6\mu\text{m}) > 10^{44} \text{ erg s}^{-1}$  that corresponds to  $\text{mag}(24\mu\text{m}) < 20(\text{AB})$  and therefore a detection in the MIPS  $24\mu\text{m}$  image at  $S/N > 10$ . At the position of *Ion2* no signal is detected in the MIPS  $24\mu\text{m}$  band down to  $\text{AB} \simeq 22.3$  (de Barros et al. 2016).

It is worth noting a photometric excess ( $S/N > 5$ ) in the second IRAC channel at  $4.5\mu\text{m}$  (Fig. 5), that we ascribed to possible  $\text{HeI}\lambda 10830 + \text{Pa}\gamma$  lines with rest-frame equivalent width of  $\sim 1100\text{\AA}$ . While these lines can only be observed with *JWST*, such a strong  $\text{HeI}\lambda 10830$  emission up to  $1000\text{\AA}$  equivalent width has been observed in local compact HII regions by Izotov et al. (2014) and in a local LyC emitter candidate (Verhamme et al. 2015).

Therefore we conclude that the signal observed in the *HST*/F336W band is very likely due to stellar emission; the only (unlikely) alternative would be the presence of a heavily obscured AGN, located at the center of the star-forming region and hidden by gas and dust at all wavelengths but visible in the ionizing continuum, a possibility we deem very contrived. An intrinsically faint AGN could co-exist with a dominating star formation activity that controls the transparency of the medium.

### 5.2. Constraining the burst of star formation

The measured ionizing photon production rate and the comparison with Starburst99 models (Leitherer et al. 1999) adopting instantaneous burst,  $Z = 0.004$  and Salpeter IMF, provide a stellar mass involved in the starburst event in the range

<sup>13</sup> <http://cxc.harvard.edu/>

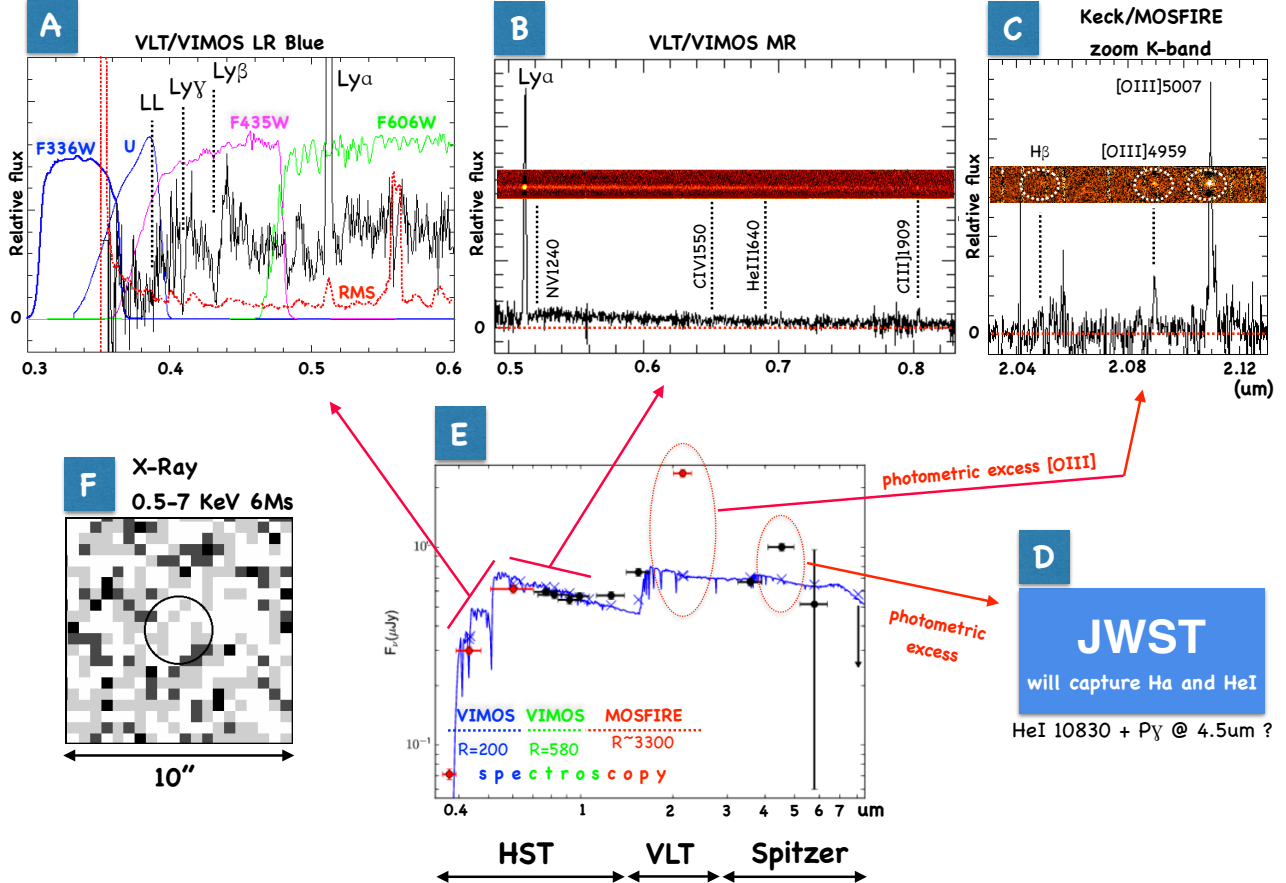


FIG. 5.— A panoramic view of the available multi-frequency data for *Ion2*, from the 0.35 to  $2.4\mu\text{m}$  wavelength range (VLT/VIMOS and Keck/MOSFIRE). Panels A, B and C: spectral coverage from U to the K-band with VLT/VIMOS and Keck/MOSFIRE. The absence of high ionization emission lines ( $\text{Nv}\lambda 1240$ ,  $\text{CIV}\lambda 1550$ ,  $\text{HeII}\lambda 1640$ ) is evident, as well as the clear detection of  $\text{Ly}\alpha$  and  $\text{CIII}\lambda 1909$  lines. The  $[\text{O III}]\lambda\lambda 4959, 5007$  lines from Keck/MOSFIRE spectrum are also shown (from de Barros et al. 2016). In panel E a schematic view of the spectral SED fitting indicating the available observations (VLT, Keck, HST, Spitzer) is shown. JWST can cover the part at  $2.4\text{-}5\mu\text{m}$ , including lines as  $\text{H}\alpha$  and  $\text{HeI}\lambda 10830$ , not accessible with current instruments (panel D). Panel F shows the 6Ms X-ray 0.5-7 keV Chandra cutout ( $10''\times 10''$ ) around *Ion2* obtained from the public Chandra observation (the circle of diameter  $3''$  marks the position of *Ion2*). The source is off-axis thus the PSF of the source would cover the entire circle symbol.

$5\times 10^6 - 5\times 10^7 \text{M}_\odot$  (depending on the IGM transmission), with the young stellar component ( $< 10\text{Myr}$ ) dominating the ionizing radiation, in which the number of O-type stars ranges between  $2\times 10^4 - 2\times 10^5$ . The ionizing photon production rate is similar to the one derived at lower redshift for a recently discovered LyC emitter (Izotov et al. 2016).

Such a young starburst event can generate substantial ionizing radiation and produce ionized cavities, and recent supernovae and stellar winds may have carved holes in the ISM that favour LyC photon escape into the intergalactic medium. It is worth stressing that the observed large  $[\text{OIII}]/[\text{OII}]$  line ratio ( $> 10$ ) is expected in this scenario (Jaskot & Oey 2013; Nakajima & Ouchi 2014). Similar large  $[\text{OIII}]/[\text{OII}]$  ratios have been observed in local starbursts (James et al. 2016) in which the younger stellar component containing O-type stars is identified in the core of the starburst (similarly to what is inferred here) and can photoionize regions out to hundreds of parsecs, as observed also in a local starburst by Annibali et al. (2015). It is worth noting that the differential depression of nebular emission among Balmer and metal lines when a substantial leakage of ionizing radiation is present could strongly affect the usual diagnostic diagrams that separate star-forming vs. AGN emission (e.g., BPT, Baldwin et al. 1981); in partic-

ular, a LyC emitter would move toward the AGN cloud if the Balmer lines are attenuated first.

## 6. CONCLUSIONS

While the LyC emitter reported here is rare among the sources with similar luminosity (Vanzella et al. 2010b; Grazian et al. 2016), the non-ionizing multi-frequency properties observed in our galaxy and the confirmed LyC emission provide valuable prospects for the characterization of similar or fainter sources in higher redshift domains. In particular, the confirmed  $z > 7.5$  galaxies (Finkelstein et al. 2013; Oesch et al. 2015; Zitrin et al. 2015) show particularly strong Oxygen and Balmer structure ( $[\text{O III}]\lambda\lambda 4959, 5007 + \text{H}\beta$ ), at the same level reported here (equivalent widths larger than  $800\text{-}1000\text{\AA}$  rest-frame). It is premature to address if those sources have effectively an  $f_{\text{esc}}(\text{LyC}) > 0$ , as optical line ratios are needed to perform a direct comparison and this is postponed until JWST launch. Our result is currently a unique high-redshift reference, both in terms of large Oxygen line ratio and large line equivalent width, and needs to be extended to statistically significant samples, especially investigating the faint luminosity domain. It also outlines the feasibility of the identification of ionizing sources during the reionization epoch.

We thank F. Annibali and D. Schaefer for useful discussions. Part of this work has been funded through the INAF

grants (PRIN INAF 2012). MB acknowledges support from the FP7 Grant “eEASy” (CIG 321913).

#### REFERENCES

Annibali, F., Tosi, M., Pasquali, A., et al. 2015, ArXiv e-prints, arXiv:1505.05545

Baldwin, J. A., Phillips, M. M., & Terlevich, R. 1981, PASP, 93, 5, 5

J. Biretta and S. Baggett, 2013, STScI, Instrument Science Report WFC3 2013-12, <http://www.stsci.edu/hst/wfc3/documents/ISRs>

Borthakur, S., Heckman, T. M., Leitherer, C., & Overzier, R. A. 2014, Science, 346, 216, 216

Bouwens, R. J., Illingworth, G. D., Oesch, P. A., et al. 2015, ApJ, 811, 140, 140

Cappelluti, N., Comastri, A., Fontana, A., Zamorani, G., Amorin, R., Castellano, M., et al., 2015, ApJ, submitted

Casertano, S., de Mello, D., Dickinson, M., et al. 2000, AJ, 120, 2747, 2747

Cen, R., & Kimm, T. 2015, ApJ, 801, L25, L25

de Barros, S., Vanzella, E., Amorín, R., et al. 2016, A&A, 585, A51, A51

Feltre, A., Charlot, S., & Gutkin, J. 2016, MNRAS, 456, 3354, 3354

Finkelstein, S. L., Papovich, C., Dickinson, M., et al. 2013, Nature, 502, 524, 524

Giallongo, E., Grazian, A., Fiore, F., et al. 2015, A&A, 578, A83, A83

Georgakakis, A., Aird, J., Buchner, J., et al. 2015, MNRAS, 453, 1946, 1946

Giavalisco, M., Ferguson, H. C., Koekemoer, A. M., et al. 2004, ApJ, 600, L93, L93

Gonzaga, S., & et al. 2012,

Grazian, A., Giallongo, E., Gerbasi, R., et al. 2016, A&A, 585, A48, A48

Grogan, N. A., Kocevski, D. D., Faber, S. M., et al. 2011, ApJS, 197, 35, 35

Inoue, A. K., Shimizu, I., Iwata, I., & Tanaka, M. 2014, MNRAS, 442, 1805, 1805

Izotov, Y. I., Orlitová, I., Schaefer, D., et al. 2016, Nature, 529, 159D160, 159D160

Izotov, Y. I., Thuan, T. X., & Guseva, N. G. 2014, MNRAS, 445, 778, 778

James, B. L., Auger, M., Aloisi, A., Calzetti, D., & Kewley, L. 2016, ApJ, 816, 40, 40

Jaskot, A. E., & Oey, M. S. 2013, ApJ, 766, 91, 91

Leitherer, C., Schaefer, D., Goldader, J. D., et al. 1999, ApJS, 123, 3, 3

Lusso, E., Comastri, A., Simmons, B. D., et al. 2012, MNRAS, 425, 623, 623

Maseda, M. V., van der Wel, A., Rix, H.-W., et al. 2014, ApJ, 791, 17, 17

Mostardi, R. E., Shapley, A. E., Nestor, D. B., et al. 2013, ApJ, 779, 65, 65

Mostardi, R. E., Shapley, A. E., Steidel, C. C., et al. 2015, ApJ, 810, 107, 107

Nakajima, K., & Ouchi, M. 2014, MNRAS, 442, 900, 900

Nestor, D. B., Shapley, A. E., Kornei, K. A., Steidel, C. C., & Siana, B. 2013, ApJ, 765, 47, 47

Oesch, P. A., van Dokkum, P. G., Illingworth, G. D., et al. 2015, ApJ, 804, L30, L30

Panessa, F., Bassani, L., Cappi, M., et al. 2006, A&A, 455, 173, 173

Peng, C. Y., Ho, L. C., Impey, C. D., & Rix, H.-W. 2010, AJ, 139, 2097, 2097

Prochaska, J. X., O’Meara, J. M., & Worseck, G. 2010, ApJ, 718, 392, 392

Rafelski, M., Teplitz, H. I., Gardner, J. P., et al. 2015, AJ, 150, 31, 31

Schlafly, E. F., & Finkbeiner, D. P. 2011, ApJ, 737, 103, 103

Siana, B., Teplitz, H., Colbert, J., et al., 2007, ApJ, 668, 62

Siana, B., Teplitz, H. I., Ferguson, H. C., et al. 2010, ApJ, 723, 241, 241

Siana, B., Shapley, A. E., Kulas, K. R., et al. 2015, ApJ, 804, 17, 17

Skelton, R. E., Whitaker, K. E., Momcheva, I. G., et al. 2014, ApJS, 214, 24, 24

Stark, D. P., Richard, J., Siana, B., et al. 2014, MNRAS, 445, 3200, 3200

Stern, D. 2015, ApJ, 807, 129, 129

Teplitz, H. I., Rafelski, M., Kurczynski, P., et al. 2013, AJ, 146, 159, 159

Ueda, Y., Hashimoto, Y., Ichikawa, K., et al. 2015, ApJ, 815, 1, 1

Vanzella, E., Siana, B., Cristiani, S., & Nonino, M. 2010a, MNRAS, 404, 1672, 1672

Vanzella, E., Giavalisco, M., Inoue, A. K., et al. 2010b, ApJ, 725, 1011, 1011

Vanzella, E., Guo, Y., Giavalisco, M., et al. 2012, ApJ, 751, 70, 70

Vanzella, E., de Barros, S., Castellano, M., et al. 2015, A&A, 576, A116, A116

Verhamme, A., Orlitová, I., Schaefer, D., & Hayes, M. 2015, A&A, 578, A7, A7

Wise, J. H., Demchenko, V. G., Halicek, M. T., et al. 2014, MNRAS, 442, 2560, 2560

Zitrin, A., Labbé, I., Belli, S., et al. 2015, ApJ, 810, L12, L12